

Stochastic bifurcation analysis of Rayleigh–Bénard convection

DANIELE VENTURI¹, XIAOLIANG WAN²
AND GEORGE EM KARNIADAKIS^{3†}

¹Department of Energy, Nuclear and Environmental Engineering, University of Bologna,
viale del Risorgimento 2, 40136 Bologna, Italy

²Department of Mathematics, Louisiana State University, 226 Lockett Hall, Baton Rouge,
LA 70803-4918, USA

³Division of Applied Mathematics, Brown University, 182 George Street, Providence, RI 02912, USA

(Received 14 April 2009; revised 23 November 2009; accepted 27 November 2009)

Stochastic bifurcations and stability of natural convection within two-dimensional square enclosures are investigated by different stochastic modelling approaches. Deterministic stability analysis is carried out first to obtain steady-state solutions and primary bifurcations. It is found that multiple stable steady states coexist, in agreement with recent results, within specific ranges of Rayleigh number. Stochastic simulations are then conducted around bifurcation points and transitional regimes. The influence of random initial flow states on the development of supercritical convection patterns is also investigated. It is found that a multi-element polynomial chaos method captures accurately the onset of convective instability as well as multiple convection patterns corresponding to random initial flow states.

1. Introduction

It has been recently found that the Oberbeck–Boussinesq approximation to convection can lead to multiple stationary states (Gelfgat, Bar-Yoseph & Yarin 1999; Gelfgat & Bar-Yoseph 2004) that are physically realizable (Pallares, Grau & Giralt 1999; Pallares *et al.* 2001). Significant research activity therefore has focused on the identification of these multiple solutions to natural convection (Puigjaner *et al.* 2004, 2008; Bousset, Lyubimov & Sedel'nikov 2008) but a systematic analysis of flow state multiplicity corresponding to appropriate initial conditions is still lacking. In fact, depending on the initial flow state – which is usually unknown in most practical applications – the transient dynamics governed by nonlinear convection equations could lead to different stationary stable convection patterns. In addition, even for well-known initial flow states, the uncertainty in boundary conditions and/or in thermophysical parameters such as the thermal diffusivity or the kinematic viscosity can introduce a significant variation in the flow pattern, especially near bifurcations (e.g. branch points, Hopf bifurcations, etc.). This lack of precise knowledge about the system however has been traditionally neglected in numerical investigations of convective heat transfer where physical parameters, boundary conditions, geometry and initial conditions are usually set to be deterministic. Further developments towards physically relevant results obviously raise the need to account for more realistic

† Email address for correspondence: gk@dam.brown.edu

operating conditions, eventually represented in terms of random variables, random processes and random fields. Recent rapid advances in the numerical solution of stochastic partial differential equations (Ghanem & Spanos 1998; Xiu & Karniadakis 2002) and application to computational fluid dynamics (Lucor *et al.* 2003; Xiu & Karniadakis 2003) open this possibility and allow the integration and the propagation of randomness in numerical simulations of convection (Le Maître *et al.* 2005; Wan & Karniadakis 2006*b*; Ganapathysubramanian & Zabarar 2007).

The purpose of the present paper is to study the stochastic bifurcation process in Rayleigh–Bénard convection within two-dimensional square enclosures. Specifically, we will consider the onset of convective instability and multiple stable steady states arising within specific ranges of Rayleigh and Prandtl numbers. The choice to rely on this simple prototype convection problem is mainly motivated by the fact that it exhibits many dynamical features of three-dimensional flows and it can be effectively treated with different stochastic approaches. In order to conduct these studies on a systematic basis we first obtain steady-state solutions and primary bifurcations through deterministic linear stability analysis and well-established parameter continuation techniques (Allgower & Georg 1990). Subsequently, we consider two different types of *random* flows. The first one corresponds to a random Rayleigh number that includes the onset of convective instability (Asokan & Zabarar 2005), i.e. we study the stochastic convection near the onset. Random Rayleigh number flows arise, for instance, when an unknown temperature difference is used as a scaling factor for the temperature distribution within the cavity. The quantification of stochastic aspects of this bifurcation problem is an important issue since any stochastic simulation of fluid mechanics can potentially include this type of branch point.

The second part of the paper is devoted to the study of multiple stable steady states arising in thermal convection within specific ranges of Rayleigh and Prandtl numbers. In particular, we will investigate the influence of initial conditions on the development of supercritical convection patterns, i.e. we attempt to analyse the flow state multiplicity beyond making just statements about its existence. We will consider, in particular, the following general question: *What is the probability that a specific convection pattern develops within the cavity if the initial flow condition is random?* As we will see, the first step in obtaining an answer to this question is to provide a suitable representation of the initial condition ensemble. In general, this involves an infinite number of degrees of freedom. In this paper, however, we will restrict our attention to a *specific class* of initial states obtained as a superimposition of particular types of low-wavenumber eddies. We first determine the basins of attraction of the steady-state convection patterns through deterministic analysis. Subsequently, we investigate random flow and heat transfer for random initial conditions intersecting different basins of attraction. Obviously, this problem has a discontinuity within the ensemble of solutions since the continuous ensemble of initial states is asymptotically split into as many parts as the number of stationary stable states. Different stochastic approaches will be considered throughout the paper for the study of both random Rayleigh number flows and random initial condition flows. In particular, we will apply generalized polynomial chaos (gPC) (Xiu & Karniadakis 2002, 2003), multi-element generalized polynomial chaos (ME-gPC) (Wan & Karniadakis 2005, 2006*a*) and Monte Carlo (MC) (Hammersley & Handscomb 1967; Fishman 1996) methods.

The paper is organized as follows. In §2 we consider the Oberbeck–Boussinesq approximation to convection via the vorticity transport equations in streamfunction-only

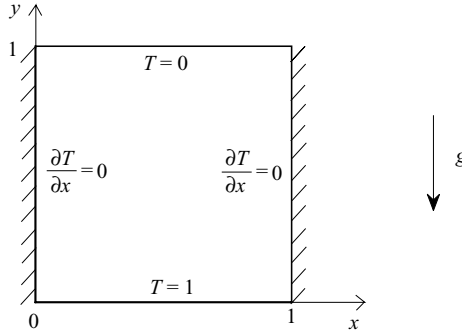


FIGURE 1. Schematic of dimensionless geometry and temperature boundary conditions. The sidewalls of the cavity are assumed to be adiabatic while the horizontal walls are kept at constant temperature. The velocity boundary conditions are of no-slip type, i.e. $\partial\psi/\partial x = 0$ and $\partial\psi/\partial y = 0$ at the walls.

formulation (Leal, Machado & Cotta 2000; Alves, Cotta & Pontes 2002) and obtain an integral representation which is the basis of the subsequent bifurcation analysis presented in §3. In §4 we investigate the onset of convective instability and determine the statistics of random Rayleigh number flows that include this bifurcation point. Section 5 is devoted to the study of multiple steady states arising in natural convection within specific ranges of Rayleigh and Prandtl numbers. In particular, we try to determine when and how each stable flow pattern is physically realized from specific deterministic initial conditions. We also consider random initial condition flows that intersect the basin of attraction of different stable states and we determine the time-asymptotic statistics of the corresponding mixture of convection patterns. In other words, we assess the probability that different supercritical flows are developed when the initial flow condition is random. The main findings and their implications are summarized in §6. We also include two appendices dealing with temperature and velocity mathematical representations.

2. Governing equations

Let us consider the dimensionless form of Oberbeck–Boussinesq approximation via the vorticity transport equation in streamfunction-only formulation

$$-\frac{\partial(\nabla^2\psi)}{\partial t} - \frac{\partial\psi}{\partial y} \frac{\partial(\nabla^2\psi)}{\partial x} + \frac{\partial\psi}{\partial x} \frac{\partial(\nabla^2\psi)}{\partial y} = -Pr\nabla^4\psi + RaPr \frac{\partial T}{\partial x}, \quad (2.1a)$$

$$\frac{\partial T}{\partial t} + \frac{\partial\psi}{\partial y} \frac{\partial T}{\partial x} - \frac{\partial\psi}{\partial x} \frac{\partial T}{\partial y} = \nabla^2 T, \quad (2.1b)$$

where $\psi(x, y, t)$ denotes the dimensionless streamfunction, $T(x, y, t)$ the dimensionless temperature while Ra and Pr are the Rayleigh and the Prandtl numbers, respectively. All the quantities have been made dimensionless by scaling lengths with the side length of the cavity L , streamfunction with the kinematic viscosity ν , time with L^2/ν and temperature with the uniform temperature difference between the horizontal walls. The boundary conditions associated with the system (2.1) are shown in figure 1 together with a sketch of the geometry. It is convenient to transform the non-homogeneous boundary condition for the temperature at the lower horizontal wall

into a homogeneous one. This is easily achieved by defining

$$T^*(x, y, t) \stackrel{\text{def}}{=} T(x, y, t) + (y - 1). \tag{2.2}$$

A substitution of (2.2) into (2.1) yields the system

$$-\frac{\partial (\nabla^2 \psi)}{\partial t} - \frac{\partial \psi}{\partial y} \frac{\partial (\nabla^2 \psi)}{\partial x} + \frac{\partial \psi}{\partial x} \frac{\partial (\nabla^2 \psi)}{\partial y} = -Pr \nabla^4 \psi + RaPr \frac{\partial T^*}{\partial x}, \tag{2.3a}$$

$$\frac{\partial T^*}{\partial t} + \frac{\partial \psi}{\partial y} \frac{\partial T^*}{\partial x} - \frac{\partial \psi}{\partial x} \frac{\partial T^*}{\partial y} + \frac{\partial \psi}{\partial x} = \nabla^2 T^*, \tag{2.3b}$$

where all the boundary conditions are the same as those in figure 1, except that now $T^* = 0$ at the lower horizontal wall.

2.1. *Integral representation*

For the purpose of the subsequent bifurcation analysis it is useful to transform the system of (2.3) into an integral form. To this end, we consider an expansion of temperature and velocity fields in terms of globally defined normalized eigenfunctions $\widehat{\psi}_n(x, y)$ and $\widehat{\Gamma}_m(x, y)$ obtained in Appendices A and B, as follows:

$$\psi(x, y, t) = \sum_{n=1}^{N_v} a_n(t) \widehat{\psi}_n(x, y), \tag{2.4a}$$

$$T^*(x, y, t) = \sum_{m=1}^{N_t} b_m(t) \widehat{\Gamma}_m(x, y). \tag{2.4b}$$

The advantage of using such representations is that they automatically satisfy all the boundary conditions as well as the continuity equation (Cotta 1993; Leal *et al.* 2000). A substitution of (2.4) into (2.3) and subsequent Galerkin projection onto $\widehat{\psi}_k$ and $\widehat{\Gamma}_k$, respectively, gives the following system of ordinary differential equations (repeated indices are summed unless otherwise stated):

$$-\frac{da_n(t)}{dt} \mathcal{A}_{nk} = a_n(t) a_m(t) \mathcal{B}_{nmk} - Pra_n(t) \mathcal{C}_{nk} + RaPr b_n(t) \mathcal{D}_{nk}, \tag{2.5a}$$

$$\frac{db_k(t)}{dt} = -a_n(t) b_m(t) \mathcal{E}_{nmk} - a_n(t) \mathcal{F}_{nk} - \gamma_k^2 b_k(t), \tag{2.5b}$$

where the coefficients \mathcal{A}_{nk} , \mathcal{B}_{nmk} , etc., are defined as

$$\begin{aligned} \mathcal{A}_{nk} &\stackrel{\text{def}}{=} \int_0^1 \int_0^1 \nabla^2 \widehat{\psi}_n \widehat{\psi}_k \, dx \, dy, & \mathcal{C}_{nk} &\stackrel{\text{def}}{=} \int_0^1 \int_0^1 \nabla^4 \widehat{\psi}_n \widehat{\psi}_k \, dx \, dy, \\ \mathcal{D}_{nk} &\stackrel{\text{def}}{=} \int_0^1 \int_0^1 \frac{\partial \widehat{\Gamma}_n}{\partial x} \widehat{\psi}_k \, dx \, dy, & \mathcal{F}_{nk} &\stackrel{\text{def}}{=} \int_0^1 \int_0^1 \frac{\partial \widehat{\psi}_n}{\partial x} \widehat{\Gamma}_k \, dx \, dy, \\ \mathcal{B}_{nmk} &\stackrel{\text{def}}{=} \int_0^1 \int_0^1 \left(\frac{\partial \widehat{\psi}_n}{\partial y} \frac{\partial \nabla^2 \widehat{\psi}_m}{\partial x} - \frac{\partial \widehat{\psi}_n}{\partial x} \frac{\partial \nabla^2 \widehat{\psi}_m}{\partial y} \right) \widehat{\psi}_k \, dx \, dy, \\ \mathcal{E}_{nmk} &\stackrel{\text{def}}{=} \int_0^1 \int_0^1 \left(\frac{\partial \widehat{\psi}_n}{\partial y} \frac{\partial \widehat{\Gamma}_m}{\partial x} - \frac{\partial \widehat{\psi}_n}{\partial x} \frac{\partial \widehat{\Gamma}_m}{\partial y} \right) \widehat{\Gamma}_k \, dx \, dy. \end{aligned}$$

Also, in (2.5b) γ_k^2 denote the eigenvalues of the Helmholtz equation (see Appendix A). The system (2.5) can be integrated in time in order to obtain the functions $a_n(t)$ and

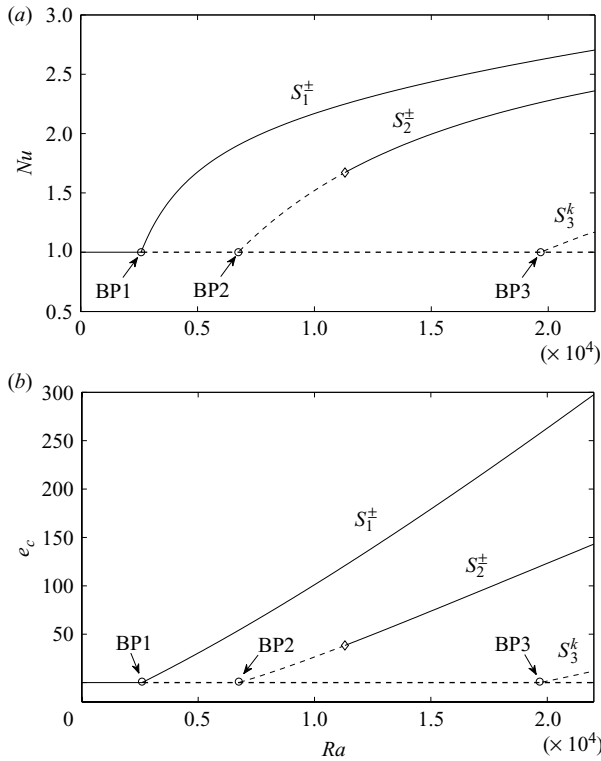


FIGURE 2. Bifurcation diagrams for natural convection of air ($Pr = 0.7$) within the cavity. Shown are the heat transfer correlation function (a) and the dimensionless kinetic energy of the fluid (b). Stable steady states are denoted by continuous lines (—) while unstable steady states are denoted by dashed lines (---). Also shown are branch points BP1, BP2 and BP3 reported in table 1.

$b_m(t)$. Once these are known, the streamfunction and the temperature fields can be easily recovered from (2.4) and (2.2).

3. Bifurcation diagrams and stability analysis

The study of bifurcations and stability of steady-state convection within the cavity has been carried out through the nonlinear system (2.5) with parameter continuation techniques. Specifically, the continuation algorithm employed to track steady states uses a prediction–correction scheme based on the Moore–Penrose matrix pseudoinverse. Mathematical details may be found in Dhooge, Govaerts & Kuznetsov (2003) (see also Allgower & Georg 1990). The bifurcation diagrams we obtained are shown in figure 2 for flows up to Rayleigh number 22 000. Figure 2(a) reports the integrated Nusselt number along horizontal walls versus the Rayleigh number, i.e. the heat transfer correlation function at Prandtl number 0.7. Figure 2(b) shows the kinetic energy of the fluid within the cavity versus the Rayleigh number, again at Prandtl number 0.7. Let us briefly explain the meaning of these diagrams. We observe a transition from conduction to convection (onset of convective instability) at Rayleigh number 2585.02 through a pitchfork bifurcation. The stable branch departing from this first branch point, denoted as BP1 in figure 2, is associated with a one-roll convection pattern defined as S_1^\pm (+ clockwise roll, – anticlockwise roll). The velocity

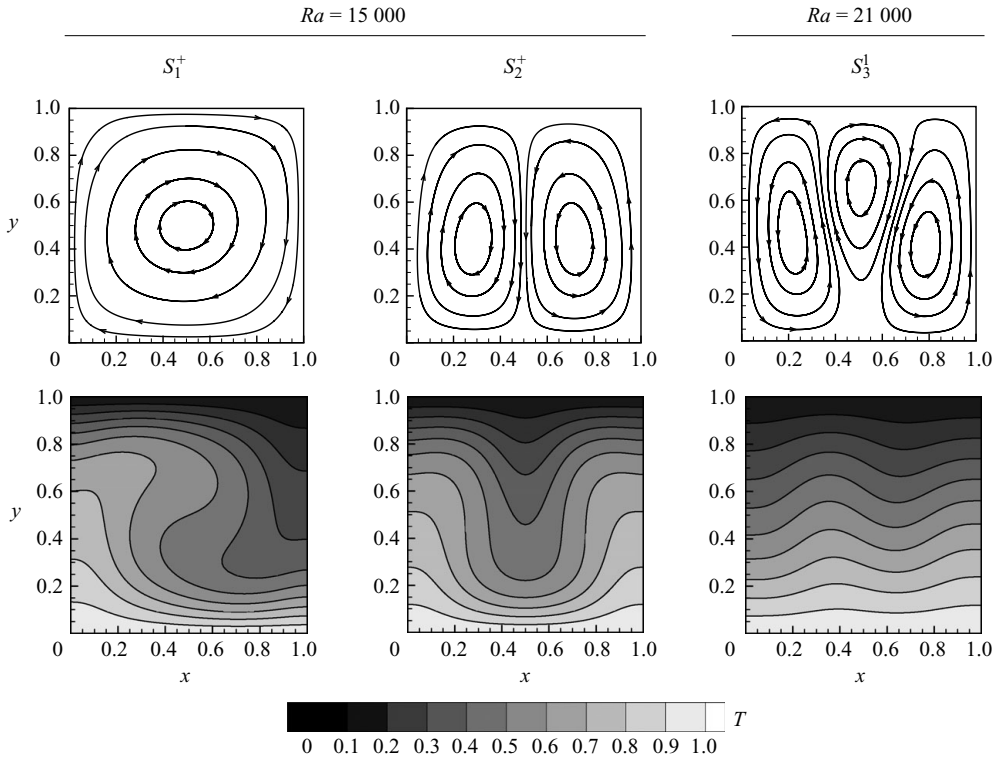


FIGURE 3. Velocity streamlines (first row) and isocontours of temperature fields (second row) of steady-state convection patterns S_1^+ (left), S_2^+ (centre) and S_3^1 (right). Both S_1^+ and S_2^+ are stable at $Ra = 15\,000$ while S_3^1 is unstable at $Ra = 21\,000$.

streamlines and the temperature field of S_1^+ are shown in figure 3 (left) at $Ra = 15\,000$. The continuation of the conduction state beyond BP1 shows something interesting. We get a secondary branch point (BP2) at $Ra = 6742.31$, with two other initially unstable stationary states defined as S_2^\pm arising from BP2. The convection pattern associated with S_2^\pm is a two-roll pattern. In figure 3 (centre) we show the velocity streamlines and the temperature field of S_2^+ at $Ra = 15\,000$. As has been pointed out by Puigjaner *et al.* (2004) this second primary bifurcation (BP2) cannot be predicted by the method proposed by Catton (1972). The initially unstable stationary states S_2^\pm become stable at Rayleigh number $Ra = 11\,279$. This means that four stable convective states S_1^\pm and S_2^\pm coexist within the range $Ra = 11\,279$ – $22\,000$, the final asymptotic pattern depending on the initial flow condition within the cavity. These four different types of flows also satisfy several *discrete* symmetries discussed in §3.1. The continuation of the conduction solution beyond BP2 leads to a third branch point (BP3) at $Ra = 19\,634$. This bifurcation yields four additional unstable three-roll flows defined as S_3^k , ($k = 1, \dots, 4$). In figure 3 (right) we show S_3^1 at $Ra = 21\,000$. The other three patterns (i.e. S_3^2 , S_3^3 and S_3^4) may be obtained from S_3^1 through the application of the discrete symmetry transformations reported in §3.1.

It is interesting to note that the sequence of bifurcations shown in figure 2 is very similar to that one reported by Puigjaner *et al.* (2004), who considered the more challenging natural convection problem in a cubical cavity with adiabatic sidewalls (Pallares *et al.* 1999, 2001, see also Puigjaner *et al.* 2008). In particular, there is a

	8 × 8	10 × 10	20 × 20	30 × 30
BP1	2585.37	2585.17	2585.03	2585.02
BP2	6745.17	6743.47	6742.35	6742.31
BP3	19 652.71	19 641.77	19 634.33	19 634.01

TABLE 1. Convergence of critical Rayleigh number at which bifurcation from conduction state occurs as a function of the number of basis functions along the x and y direction employed for both velocity and temperature representation. The Prandtl number is kept at 0.7.

correspondence between the equilibrium curves of S_1^\pm , S_2^\pm and S_3^k and those defined as S1, S5 and S4 in Puigjaner *et al.* (2004), respectively. In table 1 we report convergence of the critical Rayleigh number at which bifurcation from the conduction state occurs as a function of the number of basis functions retained for both velocity and temperature representations. For the geometry and the boundary conditions shown in figure 1, it is well known (Luijckx & Platten 1981; Gelfgat 1999) that the critical Rayleigh number at the onset is $Ra_c = 2585.02$. At higher order the present study confirms that $Ra_c = 2585.02$ (see the first row of table 1).

3.1. Symmetries of steady-state convection

The steady-state Oberbeck–Boussinesq approximation to natural convection within two-dimensional cavities satisfies several *discrete* symmetries. As is well known (see e.g. Hydon 2000, 2008), these types of symmetries may be systematically determined from known non-trivial groups of continuous Lie symmetries of the field equations (2.3). However, for the geometry and the boundary conditions considered in this paper, at least two discrete symmetries may be identified directly by looking at the equations of motion without calculating the continuous symmetry group. In fact, if $[\psi(x, y), T^*(x, y)]$ is any solution to the steady-state convection problem then

$$\mathcal{G}_1 [\psi(x, y), T^*(x, y)] \stackrel{def}{=} [-\psi(1 - x, y), T^*(1 - x, y)], \tag{3.1a}$$

$$\mathcal{G}_2 [\psi(x, y), T^*(x, y)] \stackrel{def}{=} [-\psi(x, 1 - y), -T^*(x, 1 - y)] \tag{3.1b}$$

are also solutions, i.e. they satisfy the boundary conditions and the field equations. This can be easily verified by a direct calculation. The application of a symmetry transformation to any solution of the field equations yields another solution. In the present case we observe that \mathcal{G}_1 maps S_1^+ into S_1^- and both S_2^\pm into themselves. Similarly, \mathcal{G}_2 maps S_2^+ into S_2^- and both S_1^\pm into themselves. Note that an application of \mathcal{G}_1 and \mathcal{G}_2 to the flow pattern S_3^1 reported in figure 3 (right) yields three additional different unstable flows.

4. Stochastic convection near the onset

The physical mechanism leading to the first transition at BP1 (onset of convective instability) is different for a compressible gas or a liquid (Vekstein 2004). For liquids, this transition takes place when the buoyancy effects due to temperature gradients exceed the stabilizing viscous effects (Drazin & Reid 1961; Chandrasekhar 1981) or, equivalently, when the Rayleigh number exceeds a critical value that, in general, depends on the aspect ratio of the cavity and the boundary conditions

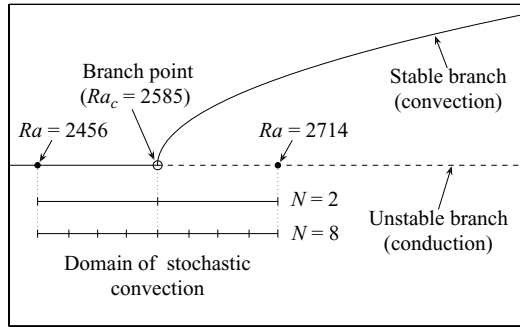


FIGURE 4. Sketch of the stochastic simulation domain for a random Rayleigh number including the onset of convective instability. Shown are also different meshes used in the ME-gPC method. Specifically, we show two subdivisions of the parameter space into $N = 2$ and $N = 8$ finite elements. Note that in each case the random element boundary is on the bifurcation point. Such a choice has been made possible by the previous deterministic bifurcation analysis.

but not on the Prandtl number. Different types of uncertainties may be considered in order to simulate natural convection flows near the onset. For instance, the thermophysical properties of the fluid may be modelled as random variables and/or the temperature distribution at the horizontal boundaries may be subject to unpredictable perturbations leading to non-uniform conditions. These random perturbations render the bifurcation process to convection *imperfect* (Ahlers, Meyer & Cannell 1989). As a consequence the pure conduction state no longer exists and a finite though perhaps very small velocity can be observed even at very small values of Rayleigh numbers. Such a *quasi-conduction* regime is typical of non-uniform temperature conditions (Kelly & Pal 1978). Realistic flows are susceptible to all these types of uncertainties. In this section however we restrict our attention to the simpler steady-state stochastic convection problem for a random Rayleigh number that includes the onset of convective instability. This very particular type of uncertainty may be associated with an unknown temperature difference between the isothermal hot and cold horizontal walls. Specifically, let us assume that the random Rayleigh number is in the form

$$Ra = Ra_c (1 + \sigma \xi), \quad (4.1)$$

where $Ra_c = 2585$ denotes the critical Rayleigh number corresponding to BP1, ξ is a normalized random variable following a uniform probability distribution in $[-1, 1]$ and σ is set to 0.05. It is easy to determine that the random Rayleigh number (4.1) approximately ranges from 2456 to 2714 (see figure 4), thus including the onset of convective instability. The only possible stable steady states in the regime around BP1 are

- (i) pure conduction for flows up to $Ra_c = 2585$;
- (ii) weak convection characterized by one-roll patterns (S_1^\pm) for $Ra > Ra_c$.

It is clear that depending on the initial condition for velocity and temperature, the temporal evolution of supercritical flows may converge either to S_1^+ or S_1^- . Such a sensitivity analysis of convection patterns as a function of the initial condition will be addressed in §5. In the present section we shall restrict our attention to steady-state flows obtained from the steady-state Oberbeck–Boussinesq approximation. In particular, we consider only one branch of the pitchfork bifurcation associated with anticlockwise one-roll flows (i.e. S_1^-) and we study the statistical ensemble

corresponding to the random Rayleigh number (4.1) through different stochastic modelling approaches (MC, gPC and ME-gPC).

4.1. Stochastic Oberbeck–Boussinesq approximation for a random Rayleigh number

Let us consider a finite-dimensional representation of the streamfunction and the temperature fields in a polynomial chaos basis $\{\Phi_i(\xi)\}$

$$\psi(x, y; \xi) = \sum_{i=0}^M \Psi_i(x, y) \Phi_i(\xi), \tag{4.2a}$$

$$T^*(x, y; \xi) = \sum_{i=0}^M \tau_i(x, y) \Phi_i(\xi). \tag{4.2b}$$

According to the standard gPC theory (Xiu & Karniadakis 2002, 2003) the basis functions $\Phi_i(\xi)$ are chosen to be Legendre polynomials of a uniform random variable. Other representations of ψ and T^* in terms of different orthogonal series are obviously possible (e.g. Le Maître *et al.* 2004). A substitution of (4.2) into the Oberbeck–Boussinesq equations (2.3) and subsequent Galerkin projection onto the basis $\{\Phi_i\}$ yields the following system of equations (only repeated indices n and m are summed):

$$-\left[\frac{\partial \Psi_n}{\partial y} \frac{\partial (\nabla^2 \Psi_m)}{\partial x} - \frac{\partial \Psi_n}{\partial x} \frac{\partial (\nabla^2 \Psi_m)}{\partial y} \right] \frac{\langle \Phi_n \Phi_m \Phi_k \rangle}{\langle \Phi_k^2 \rangle} = -Pr \nabla^4 \Psi_k + Ra_c Pr \left[\frac{\partial \tau_k}{\partial x} + \sigma \frac{\langle \Phi_1 \Phi_m \Phi_k \rangle}{\langle \Phi_k^2 \rangle} \frac{\partial \tau_m}{\partial x} \right], \tag{4.3a}$$

$$-\left[\frac{\partial \Psi_n}{\partial y} \frac{\partial \tau_m}{\partial x} - \frac{\partial \Psi_n}{\partial x} \frac{\partial \tau_m}{\partial y} \right] \frac{\langle \Phi_n \Phi_m \Phi_k \rangle}{\langle \Phi_k^2 \rangle} + \frac{\partial \Psi_k}{\partial x} = \nabla^2 \tau_k. \tag{4.3b}$$

The averaging operation $\langle \cdot \rangle$ is defined as

$$\langle f(x, y, t; \xi) \rangle \stackrel{def}{=} \int_{-1}^1 f(x, y, t; \xi) w(\xi) d\xi, \tag{4.4}$$

where f is an integrable random field and $w(\xi)$ denotes the uniform probability density function in $[-1, 1]$, i.e. $w(\xi) \equiv 1/2$. As easily seen, the averaging operation allows one to transform effectively the stochastic convection problem into a system of deterministic coupled partial differential equations to be solved for the so-called chaos modes $\Psi_i(x, y)$ and $\tau_i(x, y)$, $i = 0, \dots, M$. Once these are available it is easy to compute other quantities such as the mean and the variance of the velocity field components as

$$\langle u(x, y; \xi) \rangle = \frac{\partial \Psi_0}{\partial y}, \quad \sigma_u^2(x, y) = \sum_{k=1}^M \left(\frac{\partial \Psi_k}{\partial y} \right)^2 \langle \Phi_k^2 \rangle, \tag{4.5a}$$

$$\langle v(x, y; \xi) \rangle = -\frac{\partial \Psi_0}{\partial x}, \quad \sigma_v^2(x, y) = \sum_{k=1}^M \left(\frac{\partial \Psi_k}{\partial x} \right)^2 \langle \Phi_k^2 \rangle. \tag{4.5b}$$

If the system is subject to several different types of uncertainties that can be represented in terms of independent random variables then the multi-dimensional chaos basis $\{\Phi_i(\xi_1, \dots, \xi_n)\}$ can be constructed as a tensor product of one-dimensional basis functions. In this case, it can be proved that the total number of equations to be solved simultaneously is related to the number of independent random inputs n

and to the highest order P of one-dimensional polynomial bases by

$$M + 1 = \frac{(n + P)!}{n!P!}. \quad (4.6)$$

For the present stochastic convection problem we only have one random variable (the Rayleigh number). This means that if we represent the stochastic solution through a polynomial chaos of order $P = 6$ we have six Boussinesq-like problems to be solved *simultaneously* for the chaos modes, which actually means 12 scalar coupled partial differential equations for the temperature and the streamfunction modes. The exponential proliferation of equations predicted by (4.6) as a function of the number of random inputs n is a phenomenon known as the ‘curse of dimensionality’. Even for a moderate number of random variables the system (4.3) becomes unacceptably large and therefore several authors (e.g. Acharjee & Zabarar 2006; Burkardt, Gunsberger & Webster 2007; Doostan, Ghanem & Red-Horse 2007; Venturi, Wan & Karniadakis 2008; Ma & Zabarar 2009; see also Venturi 2006) attempted to develop new methodologies to reduce the computational complexity.

4.2. Symmetries of steady-state stochastic convection for a random Rayleigh number

A trivial calculation shows that the steady-state stochastic Oberbeck–Boussinesq approximation (4.3) for a random Rayleigh number satisfies two discrete symmetries, which are very similar to those discussed in §3.1. In particular, if

$$[\Psi(x, y), \boldsymbol{\tau}(x, y)] \stackrel{\text{def}}{=} [\{\Psi_0(x, y), \dots, \Psi_M(x, y)\}, \{\boldsymbol{\tau}_0(x, y), \dots, \boldsymbol{\tau}_M(x, y)\}] \quad (4.7)$$

denotes an arbitrary solution to the system (4.3) then

$$\mathcal{G}_1^s [\Psi(x, y), \boldsymbol{\tau}(x, y)] \stackrel{\text{def}}{=} [-\Psi(1 - x, y), \boldsymbol{\tau}(1 - x, y)], \quad (4.8a)$$

$$\mathcal{G}_2^s [\Psi(x, y), \boldsymbol{\tau}(x, y)] \stackrel{\text{def}}{=} [-\Psi(x, 1 - y), -\boldsymbol{\tau}(x, 1 - y)] \quad (4.8b)$$

are also solutions, i.e. they satisfy both the field equations and the boundary conditions. As a consequence, the statistical properties of the steady-state random flows will be influenced by the symmetries defined by the operators \mathcal{G}_1^s and \mathcal{G}_2^s . This implies, in particular, that the mean fields satisfy exactly (3.1) while the standard deviation fields can be transformed according to two different reflections with respect to $x = 0.5$ and $y = 0.5$.

4.3. Numerical results and discussion

We have determined the relevant statistics of stochastic steady-state convection for a random Rayleigh number through different stochastic approaches: MC, gPC and ME-gPC. The meshes (Wan & Karniadakis 2006a) considered for the ME-gPC stochastic simulations are shown in figure 4. Note that in each case we have put the element boundary on the bifurcation point. This has been made possible by the preliminary systematic bifurcation analysis carried out in §3. In many practical applications, however, the location of the bifurcation points may be not known *a priori*. In these cases an adaptive method (Wan & Karniadakis 2005; Ma & Zabarar 2009) is recommended to deal effectively both with discontinuities and long-term integrations. In figure 5 we show the accurate ensemble mean and ensemble standard deviation for the velocity and the temperature fields obtained by sampling 100 000 flows through the global Galerkin method outlined in §2.1. A quantitative comparison between MC, gPC and ME-gPC is reported in figure 6 where we plot the mean and the standard deviation of all the fields of interest along the crossline $y = 0.5$.

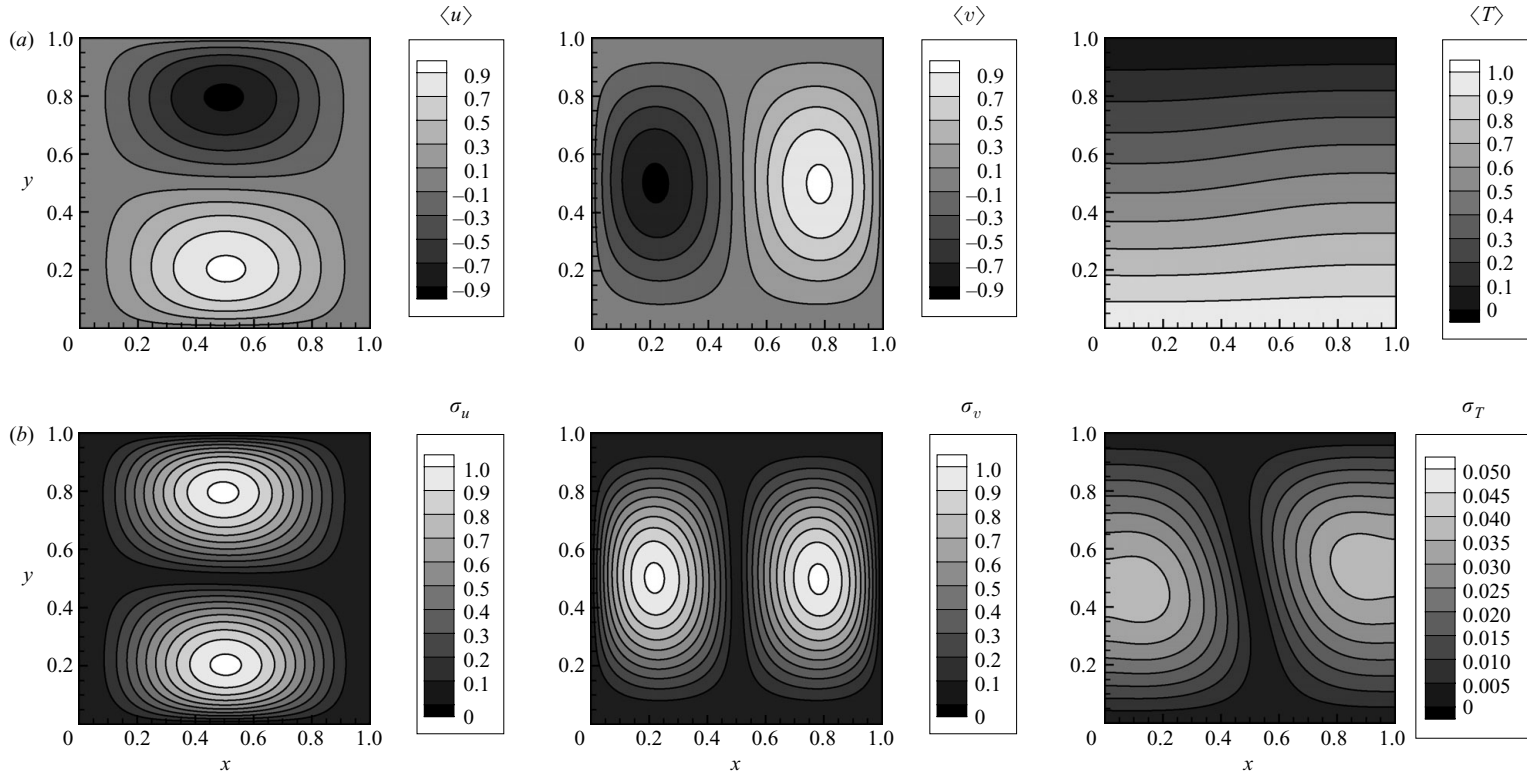


FIGURE 5. MC benchmark stochastic flow near the onset of convective instability. The flow ensemble counts 100 000 samples and it has been constructed through an accurate global Galerkin method. Shown are ensemble mean (a) and ensemble standard deviation (b) of velocity components and temperature field.

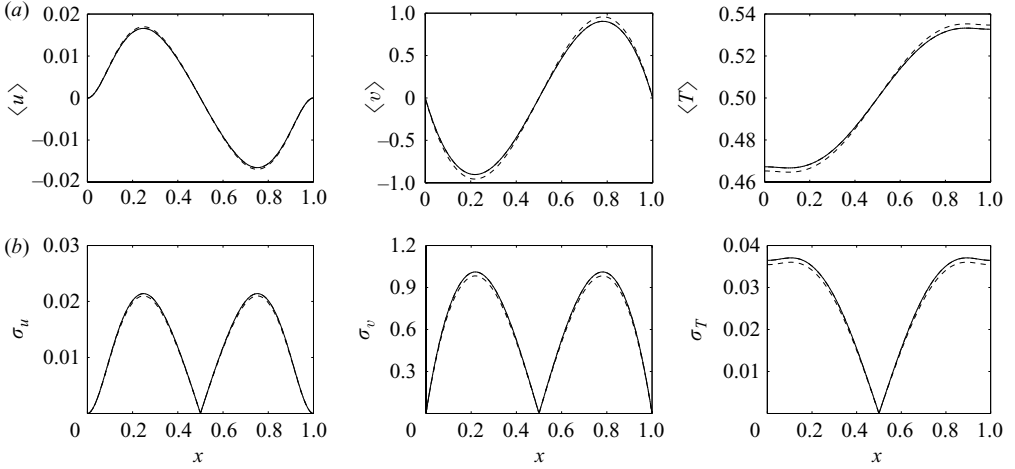


FIGURE 6. Stochastic convection near the onset. Shown are means (a) and standard deviations (b) of velocity components and temperature field along the crossline $y = 0.5$. We plot different stochastic results: MC benchmark, 100 000 samples (—), gPC order 3 (---), ME-gPC 2 elements of order 3 (···), ME-gPC 8 elements of order 3 (—·—). The ME-gPC plots are essentially superimposed on those of MC.

		gPC		ME-gPC	
		Order 3	Order 5	Two elements of order 3	Eight elements of order 3
ϵ_2	$\langle u \rangle$	2.43×10^{-2}	1.37×10^{-2}	6.53×10^{-4}	6.54×10^{-5}
	$\langle v \rangle$	2.47×10^{-2}	1.39×10^{-2}	6.62×10^{-4}	6.63×10^{-5}
	$\langle T \rangle$	1.10×10^{-3}	6.20×10^{-2}	2.97×10^{-5}	2.96×10^{-6}
	σ_u	1.29×10^{-2}	9.13×10^{-3}	5.92×10^{-4}	5.85×10^{-5}
	σ_v	1.31×10^{-2}	9.25×10^{-3}	5.99×10^{-4}	5.93×10^{-5}
	σ_T	5.73×10^{-4}	4.09×10^{-4}	2.70×10^{-5}	2.67×10^{-6}
ϵ_∞	$\langle u \rangle$	5.35×10^{-2}	3.00×10^{-2}	1.44×10^{-3}	1.44×10^{-4}
	$\langle v \rangle$	5.33×10^{-2}	2.99×10^{-2}	1.43×10^{-3}	1.43×10^{-4}
	$\langle T \rangle$	2.02×10^{-3}	1.14×10^{-3}	5.49×10^{-5}	5.43×10^{-6}
	σ_u	2.85×10^{-2}	2.01×10^{-2}	1.30×10^{-3}	1.29×10^{-4}
	σ_v	2.84×10^{-2}	1.99×10^{-2}	1.29×10^{-3}	1.28×10^{-4}
	σ_T	1.05×10^{-3}	7.52×10^{-4}	4.96×10^{-5}	5.89×10^{-6}

TABLE 2. Mean squared errors (ϵ_2) and maximum pointwise errors (ϵ_∞) of gPC and ME-gPC with respect to the MC benchmark for the stochastic convection problem near the onset.

An analysis of figure 6 shows that the gPC approach is rather accurate for the representation of both the mean and the standard deviation of velocity and temperature. Obviously, the ME-gPC results are more accurate, so accurate that the corresponding plots of figure 6 cannot be distinguished from those of MC. Therefore, in order to compare gPC and ME-gPC methods for the simulation of the onset of convective instability, we have summarized in table 2 the mean squared and the maximum pointwise errors with respect to the MC benchmark. These errors are

defined as

$$\epsilon_2 [g] \stackrel{\text{def}}{=} \left[\int_0^1 \int_0^1 (g(x, y) - g_r(x, y))^2 dx dy \right]^{1/2}, \tag{4.9a}$$

$$\epsilon_\infty [g] \stackrel{\text{def}}{=} \max_{(x,y)} |g(x, y) - g_r(x, y)|, \tag{4.9b}$$

where g is an integrable deterministic field and g_r is its reference value, in the present case that of MC. Results of table 2 confirm that the pitchfork bifurcation characterizing the transition from conduction to convection is captured rather accurately by the gPC equations (4.3), even at low-order polynomial chaos.

5. Sensitivity of multiple states to initial conditions

We have seen in §3 that different (stable) steady-state convection patterns coexist for moderate values of Rayleigh numbers, the final asymptotic state depending on the initial condition. Specifically, we have obtained a total number of four stable patterns (S_1^\pm and S_2^\pm) at Rayleigh number 15 000 and Prandtl number 0.7.

In this section we try to determine when and how each flow pattern is physically realized from specific initial conditions. In other words, we analyse the physical realizability of flow state multiplicity beyond just making statements about its existence. The first step in obtaining an answer to this question is to provide a suitable representation of the initial condition ensemble. By using the eigenfunction expansions (2.4) it is clear that any initial flow state satisfying all the boundary conditions may be represented as

$$\psi^\dagger(x, y; a_1, a_2, \dots) = \sum_{k=1}^\infty a_k \widehat{\psi}_k(x, y), \tag{5.1a}$$

$$T^\dagger(x, y; b_1, b_2, \dots) = 1 - y + \sum_{j=1}^\infty b_j \widehat{\Gamma}_j(x, y), \tag{5.1b}$$

where $\{a_k\}$ and $\{b_k\}$ are infinite sets of real Fourier coefficients. Therefore, a *complete* representation of the initial condition theoretically involves an infinite number of degrees of freedom. This suggests that the numerical determination of flow state multiplicity corresponding to arbitrary initial states can be computationally very expensive. For the purpose of the present paper we shall restrict our attention to a *specific class* of initial conditions that can be represented in terms of low-wavenumber modes. Specifically, we consider initial states in the form

$$\psi^\dagger(x, y; a_1, a_2) = a_1 \widehat{\psi}_1(x, y) + a_2 \widehat{\psi}_2(x, y), \tag{5.2a}$$

$$T^\dagger(x, y; b_2, b_4) = 1 - y + b_2 \widehat{\Gamma}_2(x, y) + b_4 \widehat{\Gamma}_4(x, y), \tag{5.2b}$$

where a_1, a_2, b_2, b_4 are assumed to be real coefficients with values in $[-1, 1]$. Obviously, (5.2a) induces a velocity field having the following representation:

$$\mathbf{u}(x, y; a_1, a_2) = a_1 \mathbf{U}_1(x, y) + a_2 \mathbf{U}_2(x, y), \tag{5.3}$$

where $\mathbf{U}_i(x, y) \stackrel{\text{def}}{=} [\partial \widehat{\psi}_i / \partial y, -\partial \widehat{\psi}_i / \partial x]$ ($i = 1, 2$) are low-wavenumber velocity modes (eddies) depicted in figure 7. The functions $\widehat{\Gamma}_2$, and $\widehat{\Gamma}_4$ appearing in (5.2) are given by (see Appendix A)

$$\begin{aligned} \widehat{\Gamma}_2(x, y) &= 2 \cos(\pi x) \sin(\pi y), \\ \widehat{\Gamma}_4(x, y) &= 2 \cos(2\pi x) \sin(\pi y). \end{aligned}$$

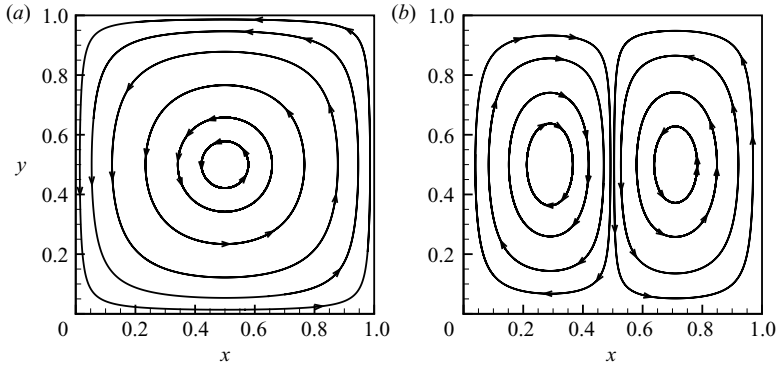


FIGURE 7. Streamlines of low-wavenumber velocity modes U_1 (a) and U_2 (b) whose combination is used to construct a random initial velocity state for flows at $Ra = 15000$ and $Pr = 0.7$.

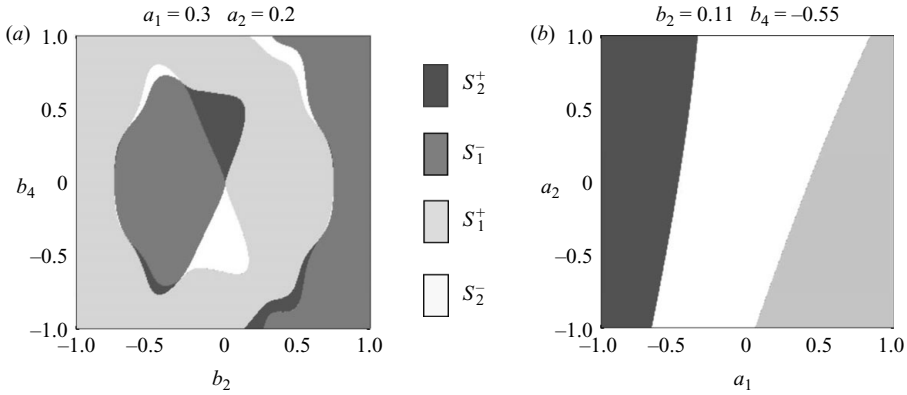


FIGURE 8. Interesting two-dimensional sections of the basins of attraction characterizing the stable flow patterns S_1^\pm and S_2^\pm at $Ra = 15000$. Numerical results show that most of the attractor is characterized by one-roll flows S_1^\pm .

The pair (U_1, \widehat{T}_2) is likely to activate one-roll stable patterns S_1^\pm , while (U_2, \widehat{T}_4) probably activates two-roll flows S_2^\pm . Obviously, other ensembles of initial states can be considered for the simulation of flow state multiplicity. In every case a fundamental question to be posed is whether stochastic approaches to convection are reliable for the representation of these multiple states.

5.1. *Attractor picture and basins of attraction*

We fix the Rayleigh number at 15000 and the Prandtl number at 0.7. From the bifurcation diagram of figure 2 we see that we have four possible stable states S_1^\pm and S_2^\pm (S_1^+ and S_2^+ are shown in figure 3). For each choice of coefficients a_1, a_2, b_2, b_4 we have an initial condition given by (5.2). By integrating the time-dependent equations (2.5) we can easily compute the time-asymptotic flow corresponding to such an initial condition. This allows us to obtain a map in a four-dimensional parameter space characterizing the basins of attraction of the stable solutions S_1^\pm and S_2^\pm . In figure 8 we plot two different sections of such a map. Let us briefly explain the meaning of these diagrams before we proceed further. If the initial condition is represented

S_1^+	S_1^-	S_2^+	S_2^-
45.8 %	45.8 %	4.2 %	4.2 %

TABLE 3. Composition of MC ensemble (160 000 flow samples) corresponding to the random initial states (5.2) at $Ra = 15\,000$ and $Pr = 0.7$. The principal components contributing to the mean flow are basically determined by one-roll stable patterns S_1^\pm . Note also that the relative contribution of S_2^\pm is equivalent to that of S_1^\mp .

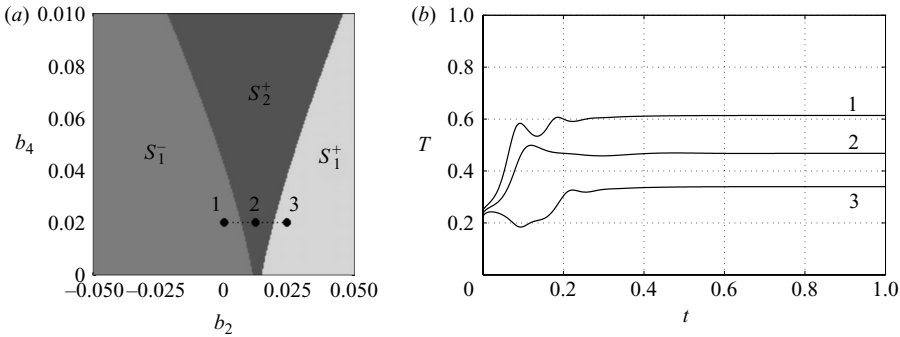


FIGURE 9. (a) Zoom-in of the basins of attraction shown in figure 8 (a), and (b) temperature time-traces at point $(x, y) = (0.75, 0.75)$ corresponding to the initial states 1, 2 and 3 indicated in (a). Note that the initial velocity condition is the same for 1, 2 and 3. The small difference between the initial temperature condition yields completely different asymptotic states.

by a set of parameters falling within the dark grey region, e.g. $(b_2, b_4) = (0, 0.4)$ in figure 8 (a), then a stable flow pattern S_2^+ develops. Similarly, if the initial state is represented by a set of parameters falling within the white regions then a flow pattern S_2^- develops. In figure 9(b) we plot several temperature time-traces at point $(x, y) = (0.75, 0.75)$ corresponding to temperature initial conditions that are nearly the same (see figure 9a). Note that such a small difference yields completely different asymptotic states. Note also that the steady-state temperatures of plots ‘2’ and ‘3’ are in agreement with temperature fields of figure 3 (left and centre). It is important to remark that even though the extension of basins of attraction associated with S_1^\pm and S_2^\pm looks comparable in figure 8, most of the attractor is characterized by one-roll stable patterns S_1^\pm . Indeed, as we will show in table 3, the overall contribution of S_2^\pm within the flow ensemble corresponding to initial conditions of type (5.2) is rather small.

5.2. Random dynamics corresponding to random initial states

In many practical applications of thermal convection we may not know precisely what are the initial conditions for the velocity and the temperature fields. We have seen that different initial conditions could lead to different stable steady states having the same Rayleigh and Prandtl numbers. In the context of stochastic fluid mechanics this flow multiplicity naturally yields two different questions. The first one concerns the determination of the time-asymptotic state corresponding to random velocity/temperature initial conditions. The second one is the random switching between different stable states under noise. In the latter case large deviation theory can be used to examine the rate of switching. In this section we look for an answer

to the following question: What is the probability that a specific convection pattern is established within the cavity if the initial condition is random? In order to answer this question we restrict our attention to a specific class of random initial states defined by (5.2), where a_1 , a_2 , b_2 and b_4 are now assumed to be independent random variables following a uniform probability distribution in $[-1, 1]$. Such an ensemble of initial conditions obviously intersects all four basins of attraction, as clearly seen in figure 8 and therefore the time-asymptotic stochastic convection will have components belonging to S_1^+ , S_1^- , S_2^+ and S_2^- . The relative contribution of each one of these states is proportional to the extension of the associated basin of attraction within the initial condition domain. A very simple measure of such an extension can be obtained through MC estimation. To this end, we have sampled 160 000 possible realizations of steady-state flows corresponding to initial condition samples in the form (5.2) and we have counted the number of each stable state appearing within the solution ensemble. The results are summarized in table 3. It is seen that the relative contribution of S_1^\pm is much bigger than that of S_2^\pm . This implies, in particular, that the principal components contributing to the mean fields are basically determined by one-roll patterns. We also note that there is an equal probability that the steady roll is clockwise or anticlockwise. In figure 10 we plot the MC ensemble mean and ensemble standard deviation for all the fields of interest. Alongside the MC method we have also employed gPC and ME-gPC approaches for the simulation of the stochastic transient dynamics corresponding to random initial states. In this case the chaos representation of the Oberbeck–Boussinesq problem takes the form

$$\frac{\partial (\nabla^2 \Psi_k)}{\partial t} + \left[\frac{\partial \Psi_n}{\partial y} \frac{\partial (\nabla^2 \Psi_m)}{\partial x} - \frac{\partial \Psi_n}{\partial x} \frac{\partial (\nabla^2 \Psi_m)}{\partial y} \right] \frac{\langle \Phi_n \Phi_m \Phi_k \rangle}{\langle \Phi_k^2 \rangle} = Pr \nabla^4 \Psi_k - Ra Pr \frac{\partial \tau_k}{\partial x}, \quad (5.4a)$$

$$\frac{\partial \tau_k}{\partial t} - \left[\frac{\partial \Psi_n}{\partial y} \frac{\partial \tau_m}{\partial x} - \frac{\partial \Psi_n}{\partial x} \frac{\partial \tau_m}{\partial y} \right] \frac{\langle \Phi_n \Phi_m \Phi_k \rangle}{\langle \Phi_k^2 \rangle} + \frac{\partial \Psi_k}{\partial x} = \nabla^2 \tau_k, \quad (5.4b)$$

where the Galerkin projection of the random initial state (5.2) onto the chaos basis $\{\Phi_k\}$ has non-trivial components. It can be shown that the steady-state solution to the system (5.4) satisfies the discrete symmetries (4.8). This implies that all the relevant statistics of the random flow such as the mean and the standard deviation will be influenced by those symmetries as well (see the discussion of §4.2). In table 4 we report the errors (4.9) of gPC and ME-gPC approaches with respect to the MC benchmark. It is seen that gPC is not accurate either for the mean or for the standard deviation fields (see also figure 11). We also note that gPC does not exhibit monotonic convergence with the polynomial chaos order; this behaviour is typical of discontinuous problems. On the contrary, low-order polynomial chaos combined with suitable ME-gPC meshes provide an efficient way to deal with discontinuities within the flow ensemble. The ME-gPC results reported in table 4 are obtained on a total number of $2^4 = 16$, $4^4 = 256$, $8^4 = 4096$ random elements.

Next, we consider local heat transfer between the horizontal walls and the fluid. This is quantified in terms of random local Nusselt number defined as

$$Nu_x \stackrel{def}{=} - \left. \frac{\partial T}{\partial y} \right|_{wall}, \quad (5.5)$$

where the subscript ‘wall’ indicates that the partial derivative is evaluated along the horizontal boundaries. The integrated Nusselt number is represented by the random

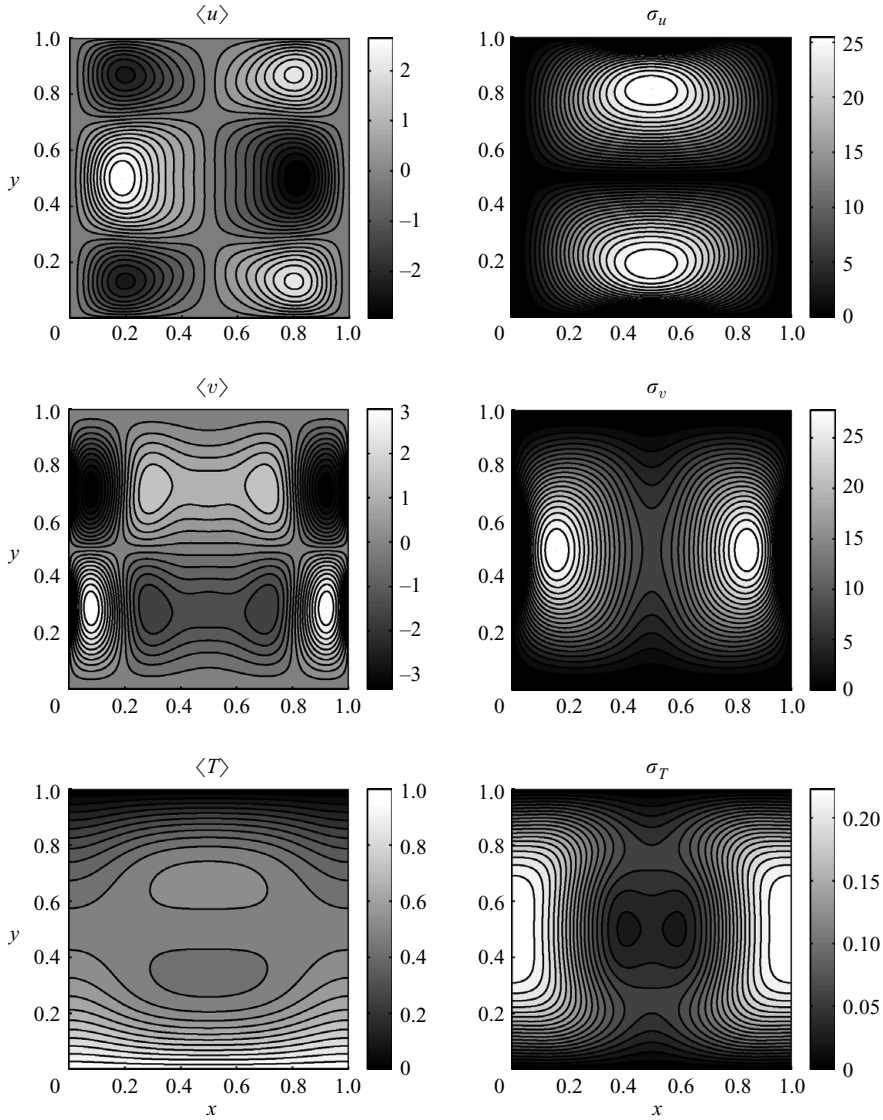


FIGURE 10. Mean and standard deviation of velocity and temperature fields corresponding to the ensemble of random initial states (5.2). Results are from MC simulation (160 000 flow samples).

variable

$$Nu \stackrel{\text{def}}{=} \int_0^1 Nu_x \, dx. \tag{5.6}$$

In figure 11 we plot the mean and the standard deviation of the random local Nusselt number along the lower horizontal wall. We observe a rather high value of the standard deviation in the proximity of the sidewalls of the cavity. This is due to the high probability that either a clockwise or an anticlockwise one-roll pattern is established. In figure 12 we show indeed that deterministic local Nusselt numbers corresponding to S_1^\pm are in very good agreement with a statistical confidence interval

		gPC			ME-gPC		
		Order 2	Order 3	Order 4	16 elements of order 3	256 elements of order 2	4096 elements of order 1
ϵ_2	$\langle u \rangle$	0.5007	0.0795	0.3054	0.0731	0.0631	0.0363
	$\langle v \rangle$	0.5346	0.0850	0.3216	0.0775	0.0666	0.0373
	$\langle T \rangle$	0.0646	0.0046	0.0345	0.0036	0.0022	0.0011
	σ_u	2.9317	0.5052	1.3168	0.4613	0.2883	0.0940
	σ_v	3.3606	1.3748	2.0111	1.3668	0.6563	0.1654
	σ_T	0.0380	0.0129	0.0274	0.0099	0.0053	0.0013
ϵ_∞	$\langle u \rangle$	1.3025	0.2448	0.7877	0.2404	0.1960	0.1149
	$\langle v \rangle$	1.4689	0.1649	0.8612	0.1588	0.1309	0.0756
	$\langle T \rangle$	0.1138	0.0121	0.0588	0.0103	0.0064	0.0024
	σ_u	5.8870	1.2208	2.5254	1.1269	0.7008	0.2166
	σ_v	7.6953	7.6359	7.6255	7.3331	2.9303	0.5943
	σ_T	0.0834	0.0565	0.0649	0.0357	0.0190	0.0043

TABLE 4. Errors in the mean and in the standard deviation of random flow obtained as superimposition of supercritical convection patterns at Rayleigh number $Ra = 15000$ ($Pr = 0.7$). Shown are mean squared errors (ϵ_2) and maximum pointwise errors (ϵ_∞) with respect to the MC benchmark flow (160 000 samples).

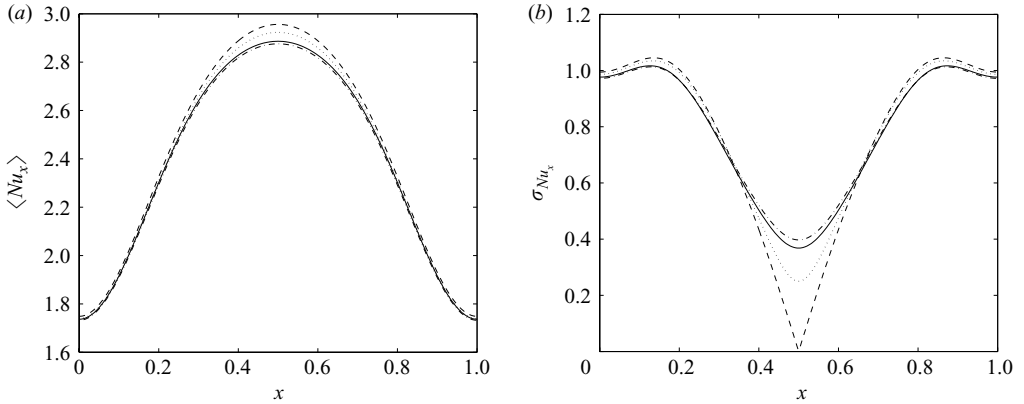


FIGURE 11. Mean (a) and standard deviation (b) of random local Nusselt number at steady state ($Ra = 15000$, $Pr = 0.7$) along the lower horizontal wall. Shown are results obtained from different stochastic approaches: MC (160 000 flow samples) (—), gPC order 3 (---), ME-gPC 256 elements of order 2 (\cdots), ME-gPC 4096 elements of order 1 (-·-).

in the proximity of the sidewalls. The mean and the standard deviation of the integrated Nusselt number (5.6) are obtained as

$$\langle Nu \rangle = 2.40, \quad \sigma_{Nu} = 0.12. \quad (5.7)$$

Note that the mean value $\langle Nu \rangle$ turns out to be in very good agreement with the deterministic integrated Nusselt number of S_1^\pm at Rayleigh number 15 000 (see figure 2). The small value of standard deviation σ_{Nu} is obviously due to the presence of several states of type S_2^\pm within the flow ensemble (see table 3).

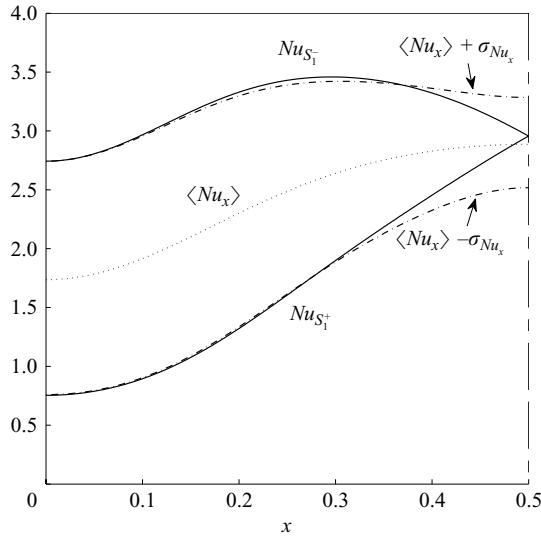


FIGURE 12. A confidence interval (—) for the random local Nusselt number along the lower horizontal wall. Also shown are the mean local Nusselt number (\cdots) and deterministic local Nusselt number corresponding to S_1^\pm (—) at Rayleigh number $Ra = 15\,000$ ($Pr = 0.7$).

6. Summary

We have investigated the effectiveness of both classical and new stochastic approaches to simulate the onset of convective instability and the influence of random initial flow states on the development of supercritical convection patterns within two-dimensional square enclosures. In order to perform this analysis we have first obtained suitable solution maps through deterministic linear stability analysis and parameter continuation techniques. Subsequently, we have considered two different sources of uncertainty. The first one corresponds to a random Rayleigh number that includes the onset of convective instability, i.e. we have studied the stochastic convection near the onset. We have found that polynomial chaos approaches applied to the streamfunction formulation of the Oberbeck–Boussinesq approximation are reliable for the representation of these types of random flows, even at low-order polynomial chaos. In the second part of the paper we have studied the problem of multiple stable steady states arising in thermal convection within specific ranges of Rayleigh numbers. Reliable stochastic convection results corresponding to the random initial condition ensemble show that the most probable convection pattern which is developed from a low-wavenumber initial state is a one-roll pattern. This type of flow, whose kinetic energy turns out to be approximately twice that associated with the two-roll pattern, is also the greatest contribution to heat transfer rate. However, the ensemble of initial states we have considered in this paper does not cover all possible initial flow conditions. For example, one may ask what is the most probable convection pattern arising from a nearly calm nearly isothermal flow within a cubical box (Stork & Müller 1972; Kirchartz & Oertel 1988; Pallares *et al.* 1996, 2001; Puigjaner *et al.* 2004, 2008) at fixed Rayleigh number. Clearly, the answer to these types of questions involves the computation of the stochastic transient corresponding to appropriate initial condition ensembles, i.e. stochastic approaches can be used to assess the probability that different convection patterns are developed in experiments.

More generally, stochastic modelling of realistic thermal convection problems has to take into account the fact that the temperature distribution at the solid boundaries may be subject to non-uniform unpredictable perturbations. These perturbations can have a significant influence both on the onset of convective instability as well as on the ensemble of supercritical states. In particular, the bifurcation process leading to convection is *imperfect* (Ahlers *et al.* 1989) and the pure conduction state no longer exists, being replaced by a *quasi-conduction* regime (Kelly & Pal 1978). In preliminary work, we have addressed this issue and modelled the random temperature perturbations as stochastic processes represented in terms of Karhunen–Loève modes (Ghanem & Spanos 1998) of a prescribed correlation kernel with finite correlation length; in contrast, the results presented here correspond to infinite correlation length. Specifically, for correlation length of the order of the cavity width we have observed stable convection patterns (not necessarily symmetric rolls) at Rayleigh number around 1000 (i.e. well below the onset of the classical deterministic case) for 1% perturbations. Further research is necessary in order to determine the influence of these non-uniform random temperature boundary conditions – parametrized by their correlation length and amplitude – on the bifurcation process.

This work was supported by OSD-MURI grant number FA9550-09-1-0613 and by DOE grant number DE-FG02-07ER25818.

Appendix A. Temperature representation

We consider an eigenfunction expansion based on the classical Helmholtz problem in Cartesian coordinates

$$\nabla^2 T^* + \gamma^2 T^* = 0 \quad (\text{A } 1)$$

with homogeneous boundary conditions

$$T^*(x, 0) = T^*(x, 1) = \frac{\partial T^*(0, y)}{\partial x} = \frac{\partial T^*(1, y)}{\partial x} = 0. \quad (\text{A } 2)$$

A straightforward separation of variables operated in (A 1) gives the following two Sturm–Liouville problems:

$$\frac{d^2 X}{dx^2} + a^2 X = 0, \quad \frac{dX(0)}{dx} = \frac{dX(1)}{dx} = 0, \quad (\text{A } 3)$$

$$\frac{d^2 Y}{dy^2} + b^2 Y = 0, \quad Y(0) = Y(1) = 0, \quad (\text{A } 4)$$

whose solutions are the well-known (Özişik 1985, 1999) normalized eigenfunctions

$$X_0(x) = 1, \quad X_n(x) = \sqrt{2} \cos(n\pi x) \quad (n = 1, 2, 3, \dots), \quad (\text{A } 5)$$

$$Y_m(y) = \sqrt{2} \sin(m\pi y) \quad (m = 1, 2, 3, \dots), \quad (\text{A } 6)$$

while the eigenvalues are

$$a_n = \pi n \quad (n = 0, 1, 2, \dots), \quad (\text{A } 7)$$

$$b_m = \pi m \quad (m = 1, 2, \dots). \quad (\text{A } 8)$$

This implies that the eigenvalues of (A 1) are

$$\gamma_{nm}^2 = \pi^2 (n^2 + m^2). \quad (\text{A } 9)$$

The temperature basis function can be written as

$$\widehat{\Gamma}_n(x, y) = X_{i(n)}(x)Y_{j(n)}(y), \tag{A 10}$$

where $i(n)$ and $j(n)$ are suitable subsequences obtained according an ordering of γ_{ij}^2 .

Appendix B. Velocity representation

All the velocity boundary conditions are of no-slip type. This means $\partial\psi/\partial x = \partial\psi/\partial y = 0$ everywhere at the boundary. In order to generate a divergence-free basis for the velocity representation satisfying such boundary conditions it is convenient (Cotta 1993; Figueira & Cotta 1996; Leal *et al.* 2000; Puigjaner *et al.* 2004) to consider the following eigenvalue problem:

$$\frac{\partial^4\psi}{\partial x^4} + \frac{\partial^4\psi}{\partial y^4} = \Lambda^4\psi, \tag{B 1}$$

$$\psi(x, 0) = \frac{\partial\psi}{\partial x} = 0, \quad \psi(x, 1) = \frac{\partial\psi}{\partial x} = 0, \tag{B 2}$$

$$\psi(0, y) = \frac{\partial\psi}{\partial y} = 0, \quad \psi(1, y) = \frac{\partial\psi}{\partial y} = 0. \tag{B 3}$$

This eigenvalue problem is symmetric and separable. The spectral theory for linear operators in a Hilbert space guarantees that the eigenfunction set is then *complete*. A substitution of

$$\psi(x, y) = X(x)Y(y) \tag{B 4}$$

into (B 1) yields two equivalent eigenvalue problems for $X(x)$ and $Y(y)$ in the form

$$\frac{d^4X}{dx^4} = \alpha^4X, \tag{B 5}$$

$$X(0) = X(1) = \frac{\partial X(0)}{\partial x} = \frac{\partial X(1)}{\partial x} = 0. \tag{B 6}$$

The general integral of (B 5) is easily found as

$$X(x) = a \sin(\alpha x) + b \cos(\alpha x) + c \sinh(\alpha x) + d \cosh(\alpha x).$$

By enforcing the boundary conditions (B 6) we get the following normalized set of eigenfunctions:

$$X_i(x) = \begin{cases} \cos[\alpha_i(x - 1/2)] / \cos[\alpha_i/2] - \cosh[\alpha_i(x - 1/2)] / \cosh[\alpha_i/2], & i = 1, 3, 5, \dots, \\ \sin[\alpha_i(x - 1/2)] / \sin[\alpha_i/2] - \sinh[\alpha_i(x - 1/2)] / \sinh[\alpha_i/2], & i = 2, 4, 6, \dots, \end{cases}$$

where the eigenvalues α_i are solutions of the transcendental equation

$$\tanh\left(\frac{\alpha_i}{2}\right) = \begin{cases} -\tan(\alpha_i/2) & \text{for } i = 1, 3, 5, \dots, \\ \tan(\alpha_i/2) & \text{for } i = 2, 4, 6, \dots \end{cases} \tag{B 7}$$

A similar solution can be obtained for $Y(y)$. A normalized basis for the two-dimensional streamfunction can be obtained as a tensor product of one-dimensional bases as

$$\widehat{\psi}_n(x, y) = X_{i(n)}(x)Y_{j(n)}(y), \tag{B 8}$$

where $i(n)$ and $j(n)$ are suitable subsequences obtained according to an eigenvalue ordering

$$\Lambda_n^4 = \alpha_{i(n)}^4 + \beta_{j(n)}^4. \quad (\text{B } 9)$$

REFERENCES

- ACHARJEE, S. & ZABARAS, N. 2006 A concurrent model reduction approach on spatial and random domains for the solution of stochastic PDEs. *Intl J. Numer. Meth. Engng.* **66** (12), 1934–1954.
- AHLERS, G., MEYER, C. W. & CANNELL, D. S. 1989 Deterministic and stochastic effects near the convective onset. *J. Stat. Phys.* **54** (5/6), 1121–1131.
- ALLGOWER, E. L. & GEORG, K. 1990 *Numerical Continuation Methods: An Introduction*. Springer.
- ALVES, L. S. DE, COTTA, R. M. & PONTES, J. 2002 Stability analysis of natural convection in porous cavities through integral transforms. *Intl J. Heat Mass Transfer* **45**, 1185–1195.
- ASOKAN, B. W. & ZABARAS, N. 2005 Using stochastic analysis to capture unstable equilibrium in natural convection. *J. Comput. Phys.* **208**, 134–153.
- BOUSSET, F., LYUBIMOV, D. V. & SEDEL'NIKOV, G. A. 2008 Three-dimensional convection regimes in a cubical cavity. *Fluid Dyn.* **43** (1), 1–8.
- BURKARDT, J., GUNSBERGER, M. & WEBSTER, C. 2007 Reduced order modelling of some nonlinear stochastic partial differential equations. *Intl J. Numer. Anal. Mod.* **4** (3–4), 368–391.
- CATTON, I. 1972 The effect of insulating vertical walls on the onset of motion in a fluid heated from below. *Intl J. Heat Mass Transfer* **15** (4), 665–672.
- CHANDRASEKHAR, S. 1981 *Hydrodynamic and Hydromagnetic Stability*. Dover.
- COTTA, R. M. 1993 *Integral Transforms in Computational Heat and Fluid Flow*. CRC Press.
- DHOOGHE, A., GOVAERTS, W. & KUZNETSOV, YU. A. 2003 MATCONT: a Matlab package for numerical bifurcation analysis of ODEs. *ACM Trans. Math. Softw.* **29**, 141–164.
- DOOSTAN, A., GHANEM, R. G. & RED-HORSE, J. 2007 Stochastic model reduction for chaos representation. *Comput. Meth. Appl. Mech. Engng* **196**, 3951–3966.
- DRAZIN, P. G. & REID, W. H. 1961 *Hydrodynamic Stability*. Cambridge University Press.
- FIGUEIRA, E. & COTTA, R. M. 1996 Benchmark results for internal forced convection through integral transformation. *Intl Commun. Heat Mass Transfer* **23** (7), 1019–1029.
- FISHMAN, G. S. 1996 *Monte Carlo: Concepts, Algorithms and Applications*. Springer.
- GANAPATHYSUBRAMANIAN, B. & ZABARAS, N. 2007 Sparse grid collocation schemes for stochastic natural convection problems. *J. Comput. Phys.* **225** (1), 652–685.
- GELFGAT, A. YU. 1999 Different modes of Rayleigh–Bénard instability in two and three-dimensional rectangular enclosures. *J. Comput. Phys.* **156**, 300–324.
- GELFGAT, A. YU. & BAR-YOSEPH, P. Z. 2004 Multiple solutions and stability of confined convective and swirling flows – a continuing challenge. *Intl J. Numer. Meth. Heat Fluid Flow* **14** (2), 213–241.
- GELFGAT, A. YU., BAR-YOSEPH, P. Z. & YARIN, A. L. 1999 Stability of multiple steady states of convection in laterally heated cavities. *J. Fluid Mech.* **338**, 315–334.
- GHANEM, R. G. & SPANOS, P. D. 1998 *Stochastic Finite Elements: A Spectral Approach*. Springer.
- HAMMERSLEY, J. M. & HANDSCOMB, D. C. 1967 *Monte Carlo Methods*. Fletcher & Son Ltd.
- HYDON, P. E. 2000 How to construct the discrete symmetries of partial differential equations. *Eur. J. Appl. Math.* **11**, 515–527.
- HYDON, P. E. 2008 *Symmetry Methods for Differential Equations: A Beginner's Guide*, 2nd edn. Cambridge University Press.
- KELLY, R. E. & PAL, D. 1978 Thermal convection with spatially periodic boundary conditions: resonant wavelength excitation. *J. Fluid Mech.* **86** (3), 433–456.
- KIRCHARTZ, K. R. & OERTEL, H., JR 1988 Three-dimensional thermal cellular convection in rectangular boxes. *J. Fluid Mech.* **192**, 249–286.
- LE MAÎTRE, O., NJAM, H. N., GHANEM, R. G. & KNIO, O. M. 2004 Uncertainty propagation using Wiener–Haar expansions. *J. Comput. Phys.* **197**, 28–57.
- LE MAÎTRE, O., REAGAN, M. T., DEBUSSCHERE, B., NAJM, H. N., GHANEM, R. G. & KNIO, O. M. 2005 Natural convection in a closed cavity under stochastic non-Boussinesq conditions. *SIAM J. Sci. Comput.* **26** (2), 375–394.

- LEAL, M. A., MACHADO, H. A. & COTTA, R. M. 2000 Integral transform solutions of transient natural convection in enclosures with variable fluid properties. *Intl J. Heat Mass Transfer* **43**, 3977–3990.
- LUCOR, D., XIU, D., SU, C.-H. & KARNIADAKIS, G. E. 2003 Predictability and uncertainty in CFD. *Intl J. Numer. Meth. Fluids* **43** (5), 485–505.
- LUIJKX, J. M. & PLATTEN, J. K. 1981 On the onset of free convection in a rectangular channel. *J. Non-Equilib. Thermodyn.* **6**, 141.
- MA, X. & ZABARAS, N. 2009 An adaptive hierarchical sparse grid collocation algorithm for the solution of stochastic differential equations. *J. Comput. Phys.* **228**, 3084–3113.
- ÖZİŞİK, M. N. 1985 *Heat Transfer: A Basic Approach*. McGraw-Hill.
- ÖZİŞİK, M. N. 1999 *Heat Conduction*, 2nd edn. Wiley-Interscience.
- PALLARES, J., ARROYO, M. P., GRAU, F. X. & GIRALT, F. 2001 Experimental laminar Rayleigh–Bénard convection in a cubical cavity at moderate Rayleigh and Prandtl numbers. *Exp. Fluids* **31** (2), 208–218.
- PALLARES, J., CUESTA, I., GRAU, F. X. & GIRALT, F. 1996 Natural convection in a cubical cavity heated from below at low Rayleigh numbers. *Intl J. Heat Mass Transfer* **39** (15), 3233–3247.
- PALLARES, J., GRAU, F. X. & GIRALT, F. 1999 Flow transitions in laminar Rayleigh–Bénard convection in a cubical cavity at moderate Rayleigh numbers. *Intl J. Heat Mass Transfer* **42**, 753–769.
- PUIGJANER, D., HERRERO, J., GIRALT, F. & SIMÓ, C. 2004 Stability analysis of the flow in a cubical cavity heated from below. *Phys. Fluids* **16** (10), 3639–3654.
- PUIGJANER, D., HERRERO, J., SIMÓ, C. & GIRALT, F. 2008 Bifurcation analysis of steady Rayleigh–Bénard convection in a cubical cavity with conducting sidewalls. *J. Fluid Mech.* **598**, 393–427.
- STORK, K. & MÜLLER, U. 1972 Convection in boxes: experiments. *J. Fluid Mech.* **54** (4), 599–611.
- VEKSTEIN, G. 2004 Energy principle for the onset of convection. *Eur. J. Phys.* **25**, 667–673.
- VENTURI, D. 2006 On proper orthogonal decomposition of randomly perturbed fields with applications to flow past a cylinder and natural convection over a horizontal plate. *J. Fluid Mech.* **559**, 215–254.
- VENTURI, D., WAN, X. & KARNIADAKIS, G. E. 2008 Stochastic low-dimensional modelling of a random laminar wake past a circular cylinder. *J. Fluid Mech.* **606**, 339–367.
- WAN, X. & KARNIADAKIS, G. E. 2005 An adaptive multi-element generalized polynomial chaos method for stochastic differential equations. *J. Comput. Phys.* **209** (2), 617–642.
- WAN, X. & KARNIADAKIS, G. E. 2006a Multi-element generalized polynomial chaos for arbitrary probability measures. *SIAM J. Sci. Comput.* **28** (3), 901–928.
- WAN, X. & KARNIADAKIS, G. E. 2006b Stochastic heat transfer enhancement in a grooved channel. *J. Fluid Mech.* **565**, 255–278.
- XIU, D. & KARNIADAKIS, G. E. 2002 The Wiener–Askey polynomial chaos for stochastic differential equations. *SIAM J. Sci. Comput.* **24** (2), 619–644.
- XIU, D. & KARNIADAKIS, G. E. 2003 modelling uncertainty in flow simulations via generalized polynomial chaos. *J. Comput. Phys.* **187**, 137–167.